Non-Invasive Determination and Monitoring
of
Free-Phase Dense Nonaqueous Phase Liquids (DNAPLs)
by
Seismic Reflection Techniques

Michael G. Waddell (mwaddell@esri.esri.sc.edu, 803-777-6484)
William J. Domoracki (bdomorac@esri.esri.sc.edu 803-777-0591)
Tom J. Temples (ttemples@esri.esri.sc.edu 803-777-3014)

Earth Sciences and Resources Institute
901 Sumter St. Room 402
University of South Carolina
Columbia, SC 29208

1.0   INTRODUCTION

Current technology for the evaluation and remediation of contaminated soil and groundwater is inadequate to meet mandated cleanup levels in a cost-effective and environmentally acceptable manner. More must be learned before realistic cleanup strategies can be developed. The technology gap comes from incomplete knowledge about the subsurface geohydrology within which various remediation technologies are applied and the inability to adequately characterize movement of pollutants. The path of contaminant movement is complex because of the interaction between earth materials and contaminants in the subsurface.

2.0   OBJECTIVE

Determination of the location and distribution of subsurface dense nonaqueous phase liquid (DNAPL) contamination poses specific challenges. Because DNAPLs are denser than groundwater the migration of these fluids in the subsurface is controlled in part by gravity such that the direction of contaminant flow is not necessarily the same as groundwater flow. Below the water table DNAPLs tend to accumulate in highly concentrated discrete layers or pools in structural lows or "sinks" above low permeability geologic layers. Furthermore, the occurrence of DNAPL in the subsurface can be highly localized and can occur at differing structural levels. Therefore, determination of the distribution of the contamination can be difficult because of missed pools of highly concentrated product. The key to maximizing the amount of DNAPL recovered from the subsurface is constructing a comprehensive and detailed picture of the geometry and spatial variations of the lithologic units comprising the subsurface. In addition, direct detection of DNAPL itself by non-invasive techniques will immensely aid remediation efforts.

Traditional methods used to determine location and extent of DNAPL contamination require point-source data obtained from invasive methods such as borehole geophysical logs and cone penetrometer data. These invasive methods not only run the risk of cross-contamination of an aquifer, but may not locate pools of contamination because of inadequate spatial coverage.

3.0   APPROACH

The seismic reflection method provides a non-invasive means to acquire spatially dense subsurface information. Typically, a two dimensional high resolution seismic reflection survey may have data points only a foot apart Vertical resolution of a typical high resolution seismic reflection survey is three to five feet. These data, combined with existing borehole information, can provide a detailed picture of the subsurface.

In addition to subsurface imaging capabilities, seismic data if properly calibrated with borehole information, can be used to map typical aquifer properties such as porosity, permeability, and clay content. This information can be integrated into two and three dimensional structural models to delineate preferential pathways for subsurface contaminant transport. Furthermore, under certain circumstances, borehole calibrated seismic reflection data can be used to infer the presence of a specific fluid within a lithologic unit. These techniques utilize the fact that a change in the fluid

content within a lithologic unit causes a change in the recorded seismic amplitude as a function of the angle of incidence of the impinging energy, i.e. the source to receiver offset distance. In the Petroleum industry these reflection amplitude-versus-offset (AVO) techniques have been used successfully for over twenty years to directly detect the presence of subsurface hydrocarbons (Ostrander, 1984; Allen and Peddy, 1993). Recently, we have used this method to delineate free phase DNAPL concentrations at a depth of 150 feet at the Savannah River Site and DOE Hanford Site (Waddell et al., 1997; 1999).

Another application of seismic reflection profiling and AVO analysis is the monitoring the effectiveness of reservoir exploitation. In this case successive seismic surveys are conducted to obtain a time-lapse image of the subsurface as the reservoir is drained. Because seismic reflection amplitude is related to the material properties of the reservoir, it is possible to monitor fluid flow. In the last several years time-lapse seismic surveys have become commonplace in the Petroleum industry to determine the effectiveness of hydrocarbon recovery methods. We have adapted time-lapse seismic surveying to monitor the efficiency of the Dynamic Underground Stripping project (DUS) at SRS. This project is ongoing.

4.0 PROJECT DESCRIPTION

Seismic reflection surveying has been used since the mid-1920s to map subsurface geology - primarily for petroleum exploration (see Waters, 1981 for an overview). However, use of the method for engineering and environmental applications did not begin in earnest until the early 1980s. The principles of reflection seismology are the same for both the petroleum and environmental fields. The major difference between the applications is scale.

In the seismic reflection method the arrival time and amplitude of elastic waves, generated by an artificial source and reflected from subsurface layers, are recorded and analyzed. The arrival time and amplitude of the reflected waves are dependent on differences in the material properties of the layers investigated (density, bulk modulus, shear modulus, Poisson's ratio), as well as the angle of incidence of the impinging energy. Usually, only compressional waves (P, longitudinal, acoustic) are recorded. For specialized applications, particularly those where information on Poisson's ratio is needed, shear waves (S, transverse) are recorded also.

The ability of seismic data to resolve geologic features is governed by the spacing of the sensors (geophones) on the surface, the frequency of the reflected signal, and the velocity structure of subsurface. Much of the terminology concerning the resolution of seismic reflection data is derived from optics. Hence, the temporal (vertical) resolution is defined as one quarter of the dominant wavelength of the data. Thus, for typical environmental surveys where the frequency of the reflected signal is 100 Hz or more and subsurface compressional wave velocities are 2000-8000 ft/s, the vertical resolution is 3-20 feet. The spatial resolution is defined by the radius of the first Fresnel zone, i.e., the area of the reflection "point". The diameter of the first Fresnel zone is dependent on the depth of the target and the wavelength of the reflected signal. For a target 200 feet deep, typical first Fresnel zone diameters are 80-150 feet. In practice, because of the center-weighted nature of the Fresnel zone, the actual spatial resolution limits are on the order of half the radius of first Fresnel zone or less. That is, for a target 200 feet deep the spatial resolution is 20-40 feet. In order to insure adequate subsurface sampling of a reflector the surface recording station spacing is usually no greater than half the radius of the first Fresnel zone of the target horizon.

Typical seismic sources for environmental seismic surveys include sledge hammer, weight drop, vibrator, and small explosive charges. Regardless of the source used, the source must be repeatable and of sufficient energy to propagate waves to the target depth. In addition, the source must be able to generate a high enough frequency signal to resolve geologic features of interest. Seismic sources such as the sledge hammer, weight drop, and vibrator operate on the land surface and often do not require special permitting.

The reflected seismic waves are picked up by transducers known as geophones. A geophone consists of a coil suspended by a damped spring in a magnetic field. It is coupled to the land surface by a 2 to 3 inch metal spike on the bottom of the geophone casing. As a seismic wave passes the geophone, the geophone casing moves and creates a voltage that is proportional to the velocity of the waves. This voltage signal is carried via a cable to a recording instrument or seismograph where it is amplified, filtered, digitized, and stored. The recorded signal is further characterized in a processing center to create a seismic profile that is a vertical time image of the subsurface layers. For a typical seismic survey several hundred geophone locations are required to ensure adequate subsurface coverage.

Most seismic reflection data are recorded using the common depth point (CDP) method. The CDP method involves designing the seismic survey such that multiple raypaths are recorded from the same subsurface reflection points. This sampling redundancy allows for determination of the gross subsurface velocity structure and the cancellation of certain types of extraneous seismic waves. In the data processing center the seismic traces that represent the same reflection points are sorted (CDP sort) into "CDP gathers". A correction is made for the source to receiver offset of the different raypaths (normal moveout or NMO correction), and the traces in the gather summed together to form a single composite trace (CDP stack). This composite trace represents the result that is obtained when the source and receiver are coincident on the surface.

Seismic reflection data acquisition can be done as either two-dimensional recording or three dimensional recording. Two dimensional seismic data are recorded where the source points and receiver locations are inline such that a profile is generated. Three dimensional seismic data are recorded where the source points are located within area.

In the 1960's petroleum companies recognized that in young sediments (Tertiary age) large seismic amplitudes were associated with gas saturated sands. However, it was soon realized that not all large seismic amplitudes represented hydrocarbon saturated sands. The normal incidence (NI) reflectivity (bright spot) techniques involved three different scenarios base upon a water saturated state and a hydrocarbon saturated state (for this discussion a sand/shale or sand/clay interface). The scenarios are classified by changes in NI reflectivity from a water saturated a gas or hydrocarbon sand. The three scenarios are:

- Dim spot- a large positive amplitude that is reduced to a smaller positive amplitude,
- Phase reversal- a small positive amplitude that changes to small negative amplitude and
- Bright spot- a negative amplitude increasing to a large negative amplitude.

The dim spot is generally associated with a large acoustic impedance contrast and is a good technique

for inferring lithology. Bright spot anomalies are generally good for interpreting lithology and estimating sand thickness. Phase reversal reflections are not generally reliable because geologic features (i.e. faults) can cause the reflections to appear to reverse phase. This does not necessarily indicate a change lithology (Vern and Hilterman, 1995). The bright spot technique was the first direct hydrocarbon indicator.

In 1984 Ostrander published a article entitled "Plane-wave reflection coefficients for gas sands at non-normal angles of incidence". Ostrander observed that the P-wave reflection coefficient at the interface between two media varies with the angle of incidence of the impinging energy. In this article Ostrander investigated the phenomenon of compressional wave reflection amplitude variation with angle of incidence and changes in Poisson's ratio. Poisson's Ratio is defined as the ratio of transverse strain to longitudinal strain; it can be expressed in terms of P-wave and S-wave velocities (1) (Sheriff, 1991).

$$\sigma = \frac{\dfrac{V_p{}^2}{V_s} - 2}{2\left(\left[\dfrac{V_p}{V_s}\right]^2 - 1\right)} \tag{1}$$

σ= Poisson's ratio
V_p= compressional wave velocity
V_s= shear wave velocity

Much of Ostrander's work was based upon Koefoed's 1955 work on determining the reflection coefficients of plane longitudinal waves reflected at a boundary between two elastic media. Koefoed observed that if there were two elastic media with the top medium having a smaller Poisson's ratio than the underlying medium, there would be an increase in the reflection coefficient with increasing angle of incidence. He also observed that if the Poisson's ratio of the lower medium was lower than the overlying medium, the opposite would occur with a decrease in the reflection coefficient with an increase in the angle of incidence. Another observation was that the relative change in reflection coefficient increases as the velocity contrast between the two media decreases. Koefoed also noted that if Poisson's ratio for both media was increased but kept equal, the reflection coefficient at the larger angles of incidence would also increase. Ostrander (1984) found that changes in Poisson ratio caused by the presence of hydrocarbons in the pore space had dramatic effect on the P-wave reflection coefficients and that these effects could be related to seismic amplitude anomalies.

In order to understand amplitude-versus-offset (AVO) techniques one has to understand offset-dependent-reflectivity. Offset-dependent-reflectivity is the variation in the reflection and transmission coefficients with incident angle (Castagna and Backus, 1993).

The following discussion describes the equations and theory used to determine the amplitude

of elastic waves for both transmission and reflection at an acoustic boundary for normal and non-normal angle incident angles, i.e. offset dependent reflectivity. Also keep in mind that the discussion is for a simplistic model and the majority of reflections observed on a seismic profile are the superposition of events from multiple layers and will have a more complex AVO response.

As implemented in the Petroleum industry, AVO analysis involves comparing modeled AVO responses with field data to find a deviation from an expected background response. The expected background response is usually taken to be a water saturated reservoir; thus, the deviation from the expected response is an indication of hydrocarbons. DNAPLs have grossly similar acoustic characteristics as liquid hydrocarbons; therefore, if DNAPL is present in free-phase in large enough quantities, similar types of analyses as those performed by the petroleum industry can be applied to directly detect the presence of DNAPL.

An understanding of reflection AVO techniques can be obtained by a review of elastic wave propagation. A P-wave incident on a boundary between two linear elastic homogeneous isotropic (LEHI) media generates four types of waves: 1) transmitted P-wave; 2) reflected P-wave; 3) reflected S-wave; 4) a transmitted S-wave (Fig. 1). The amplitudes of the reflected and transmitted waves at the boundary depend upon the P-wave and S-wave velocities, the density of the two media, and the angles of incidence and refraction, as determined from Snell's Law. The angles, with respect to the normal, of the reflected and transmittal rays are given by Snell's Law (2),

$$\rho = \frac{\sin\Theta_1}{V_{P_1}} = \frac{\sin\Theta_2}{v_{P_2}} = \frac{\sin\Theta_1}{V_{s_1}} = \frac{\sin\Theta_2}{v_{s_2}} \qquad (2)$$

V_{p1} = P-wave velocity in medium 2,
V_{s1} = S-wave velocity in medium 1,
V_{s2} = S-wave velocity in medium 2,
Θ_1 = incident P-wave angle,
Θ_2 = transmitted P-wave angle,
Φ_1 = reflected S-wave angle,
Φ_2 = transmitted S-wave angle, and
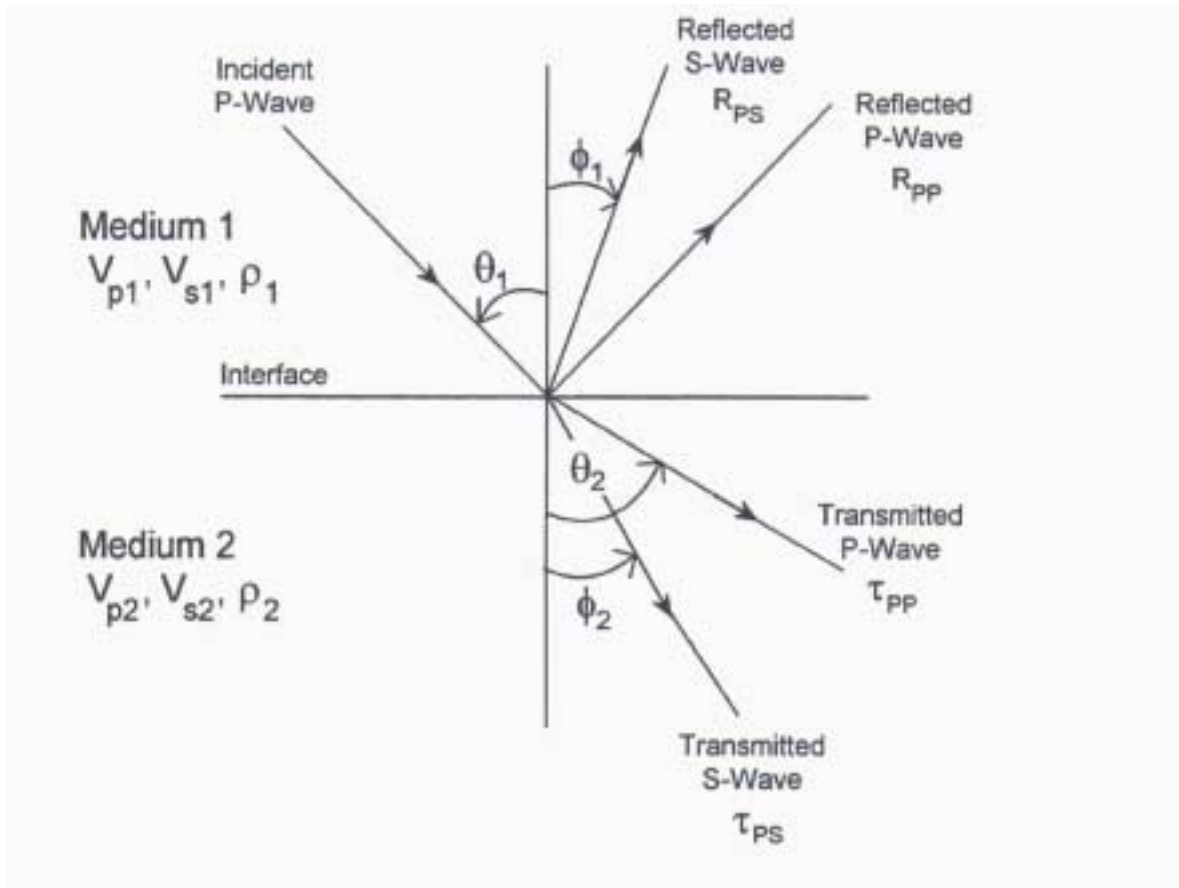ρ is the ray parameter (Fig 1).

Figure 1.   Elastic waves generated at a boundary. A P-wave incident at a angle q on a boundary between two linear elastic homogenous isotropic (LEHI) materials generates four wave types: reflected P, reflected S, transmitted P, transmitted S. The angles of reflection and refraction are governed by Snell's law from optics. The material properties of the media are described by the P-wave velocity, density, and Poisson's ratio. The S-wave velocity can be found from the P-wave velocity and Poisson's ratio.

The amplitude of the reflected and transmitted waves is described by the Zoeppritz (1919) equations (3).

<div align="right">(3)</div>

$$\begin{bmatrix} \sin\Theta_1 & \cos\Theta_1 & -\sin\Theta_2 & \cos\Theta_2 \\[6pt] -\cos\Theta_1 & \sin\Theta_1 & -\cos\Theta_2 & -\sin\Theta_2 \\[6pt] \sin2\Theta_1 & \dfrac{V_1}{W_1}\cos2\Theta_1 & \dfrac{\rho_2 W_2^2 V_1}{\rho_1 W_1^2 V_2}\sin2\Theta_2 & \dfrac{-\rho_2 W_2 V_1}{\rho_1 W_1^2}\cos2\Theta_2 \\[10pt] \cos2\Theta_1 & \dfrac{-W_1}{V_1}\sin2\Theta_1 & \dfrac{-\rho_2 V_2}{\rho_1 V_1}\cos2\Theta_2 & \dfrac{-\rho_2 W_2}{\rho_1 V_1}\sin2\Theta_2 \end{bmatrix} \begin{bmatrix} A_{RP} \\[6pt] A_{RS} \\[6pt] A_{TP} \\[6pt] A_{TS} \end{bmatrix} = \begin{bmatrix} -\sin\Theta_1 \\[6pt] -\cos\Theta_1 \\[6pt] \sin2\Theta_1 \\[6pt] -\cos2\Theta_1 \end{bmatrix}$$

where V and W are the P-wave and S-wave velocities and ρ is density.

The reflection coefficient of the P-wave as a function of the incident angle, $R_{pp}(\Theta_1)$, is defined as the ratio of the amplitude of the reflected P-wave to that of the incident P-wave (Castagna and Backus, 1993). The P-wave transmission coefficient, $T_{pp}(\Theta_1)$, is the ratio of the amplitude of the transmitted P-wave to that of the incident P-wave (Castagna and Backus, 1993). The P-wave reflection coefficient, R_p ,at normal incidence is given by the following equation:

<div align="right">(4)</div>

$$R_p = \frac{I_{p_2} - I_{p_1}}{I_p + I_p} = \frac{1}{2} * \frac{\Delta I_p}{I_{pA}} \approx \frac{1}{2} * \ln * \frac{I_{p_2}}{I_p}$$

I_{p2} = acoustic impedance of medium 2 = $\rho_2 V_{p2}$
ρ_2 = density of medium 2

I_{p1} = acoustic impedance of medium 1 = $\rho_1 V_{p1}$
ρ_1 = density of medium 1

I_{PA} = average acoustic impedance across the interface = $(I_{p2}+I_{p1})$, and
$\Delta i_p = I_{p2}-I_{p1}$.

The P-wave transmission coefficient at normal incidence T_p is given by:

<div align="center">$T_p = 1-R_p$</div>

<div align="right">(5)</div>

The complexity of the Zoeppritz equations has led to numerous approximations to simplify the calculations. Some of the approximations are Bortfield (1961), Aki and Richards (1980), and Shuey 1985. The Aki and Richards (1980) approximation to the Zoeppritz equations is given below

$$R(\theta) \cong V_p \left(\frac{\Delta P}{P}\right) + b \left(\frac{\Delta \rho}{\rho}\right) + c \left(\frac{\Delta V_S}{V_s}\right)$$
(6)

$\theta = \arcsin [(P_2 / P_1) \sin\theta_{incident}$
$a = \frac{1}{2} + \tan^2 \theta$
$b = 0.5 - [(2S^2 / P^2) \sin^2\theta$
$c = - (4S^2 / P^2) \sin^2\theta$
$V_p = (V_{p1} + V_{p2}) / 2; \quad V_p$ is P-wave velocity
$V_s = (V_{s1} + V_{s2}) / 2; \quad V_s$ is S-wave velocity
$\rho = (\rho_1 + \rho_1) / 2; \quad \rho$ is bulk density
$\Delta P = P_2 - P_1$
$\Delta S = S_2 - S_1$
$\Delta \rho = \rho_2 - \rho_1$

In this equation the reflection amplitude is expressed in three terms containing P-wave velocity, S-wave velocity, and bulk density.

The Aki and Richards equation 6, was rearranged by Shuey (1995).   In this study we used the full Zoeppritz equations, Aki and Richards modification of Zoeppritz equations and Shuey modification of Zoeppritz equations. The Shuey approximation of Zoeppritz's equations stresses the importance of Poisson's ratio as the primary determinant of the AVO response of a reflection (Allen and Peddy, 1993). Shuey's formula for the reflection coefficient (amplitude) is:

$$R\theta \approx R_0 + (A_O * R_O + \frac{\Delta \sigma}{1 - \sigma^2}) * \sin^2\theta + \frac{1}{2} * \frac{\Delta V_p}{V_p} * \tan^2\theta - \sin^2\theta$$
(7)

$$\Delta V_p = (V_{p2} - V_{p1}) \qquad\qquad \theta = (\theta_2 + \theta_1)/2$$

$$V_p = (V_{p2} + V_{p1})/2 \qquad\qquad \Delta\sigma = (\sigma_2 + \sigma_1)$$

$$\Delta V_s = (V_{s2} - V_{s1}) \qquad\qquad \sigma = (\sigma_2 + \sigma_1)/2$$

$$V_s = (V_{s2} + V_{s1})/2$$

$$\Delta\rho = (\rho_2 - \rho_1) \qquad\qquad\qquad \rho = (\rho_2 + \rho_1)/2$$

$$R_o \approx \frac{1}{2}\left(\frac{\Delta V_p}{V} + \frac{\Delta_\rho}{\rho}\right) \qquad\qquad A = A_0 + \left(\frac{1}{(1-\sigma)^2}\right)\frac{\Delta\sigma}{R_0}$$

$$A_0 = B - 2\left(1+B\right)\left(\frac{1-2\sigma}{1-\sigma}\right) \qquad\qquad B = \frac{\dfrac{\Delta V_P}{V_p}}{\dfrac{\Delta V_p}{V_p} + \dfrac{\Delta_\rho}{\rho}}$$

V_{p1} = P-wave velocity of layer one V_{p2} = P-wave velocity of layer two
V_{s1} = S-wave velocity of layer one V_{s2} = S-wave velocity of layer two
ρ_1 = Density of layer one ρ_2 = Density of layer two
σ_1 = Poisson Ratio of layer one σ_2 = Poisson Ration of layer two
θ_1 = incidence and transmission angle layer one.
θ_2 = incidence and transmission angle layer two.
R_0 = Normal incidence (NI), i.e. reflection coefficient for zero-offset.
B = is the AVO gradient.
A_0 = is the normal incidence amplitude.

NI and PR are defined as

$$NI = \frac{(\rho_2\rho_2) - (\rho_1\rho_1)}{(\rho_2\rho_2) + (\rho_1\rho_1)} = \frac{(z_2 - z_1)}{(z_2 + z_1)} \qquad\qquad z \text{ is the acoustic} \qquad (8)$$
$$\text{impedance:}$$

$$PR = \frac{\Delta\sigma}{(1-\sigma_{avg})^2} \qquad\qquad\qquad\qquad\qquad\qquad (9)$$

(Vern and Hilterman, 1995).

In the Shuey formulation, reflection AVO can be thought of a combination of normal incidence reflectivity and a far offset reflectivity, or "Poisson reflectivity", that arises primarily as a result of changes in the Poisson's ratio between media.

As previously stated, AVO analysis involves comparing modeled responses to field data to find a deviation from an expected background response. Deviations from the expected response are caused by either a change in lithology or pore fluid. Types of analysis that are routinely performed include offset range limited stacks and study of AVO gradients. Because seismic data typically contain a significant amount of random noise, studying CDP stack sections utilizing only near, middle, and far offset ranges are useful to study the reflection amplitude at small, intermediate, and large angles of incidence. Thus, a near offset stack is compared to a far offset stack from a suspected anomalous region. These stacks are compared to similar stacks from along the reflection where no anomaly is present and the modeled responses. In a like fashion, the AVO gradient, or rate of amplitude change as a function of incident angle is studied. A common analysis is to crossplot the AVO gradient versus the zero-offset amplitude for anomalous and non-anomalous zones. Clustering of points in a quadrant consistent with the model is an indication of a fluid change.

5.0   RESULTS

Savannah River Site

At the Dynamic Underground Stripping project (DUS) (Fig. 2) there are two primary types of DNAPLs present below the water table, trichloroethylene (TCE) and tetrachloroethylene (PCE). The primary objective of this project is to determine the feasibility of using high resolution reflective seismic and AVO analysis to monitor the effeteness of the DUS to remove DNAPLs.

The objective is to acquire a seismic line across the area where there are accumulations of DNAPL ("nasty" well Fig. 2). Based upon existing well data ("nasty" well and MSB-23 Fig.2) the DNAPL appears to be accumulating approximately 140 ft. below land surface. Less than a mile from this location is the M-Area seepage basin where we used surface seismic data and AVO analysis to image DNAPL at similar depths (Waddell et al., 1997). Encouraged by the results of that project, it was proposed to use surface seismic and AVO analysis to help monitor the effectiveness of the DUS.

Seismic line DUS-1 used similar acquisition parameters as the seismic lines acquired at the M-Area seepage basin (Waddell et al., 1997). The seismic data were acquired using a 120 channel seismograph, 2 feet group spacing, and a sledge hammer seismic source. Data quality in the M-Area is generally poor as can be seen on Figure 3. The only reflection present in the data occurs between shot points 189 and 269 (Fig. 3). The highest concentration of chlorinated solvents is reported in the well labeled "nasty" which located at shot point 210 on line DUS-1. Thus, it appears that the only prominent reflection occurs in the area of highest concentration of solvents.
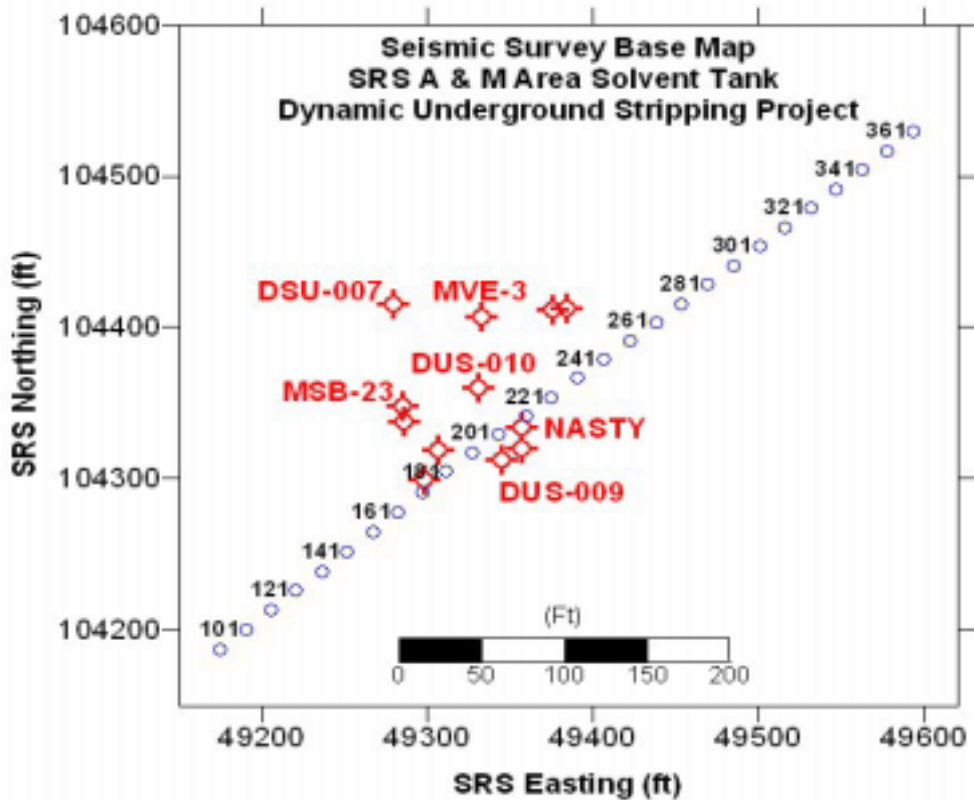
Figure 2   Location map of seismic line DUS-1 and significant wells.

Offset range limited stacking was used to investigate any AVO effects caused by the presence of DNAPL. Seismic models suggest that if DNAPL is present a significant amplitude effect should be noted on offset traces representing angles of incidence greater than 30^0.

Near and far offset stack sections were produced (Figs. 4 and 5).   The amplitude envelope (magnitude of the Hilbert transform) is plotted instead of simple trace amplitude to enhance the amplitude variations.

Limited Offset Range Stacks DUS-1

Figure 4 is the near offset stack (offsets from 1 to 113 feet). Figure 5 is the far offset stack (offsets from 113 to 240 feet). Line DUS-1 is located so that the line crosses over the highest concentrations of DNAPL ("nasty" well). If the modeling data are correct, there should not be any large amplitude anomalies present on the near offset stack (Fig. 4).   No large amplitude anomalies are noted. The modeling data indicates that the presence of DNAPL should be denoted by large

amplitude anomalies on the far offset stack. Large amplitude anomalies are noted between shot points 169 and 268 at approximately 115 ms (Fig 5) consistent with the model study. Furthermore, this anomaly is located at the depth and location of the highest concentration of DNAPL ("nasty" well at shot point 210 Fig. 2).

After the steam injection in completed, the seismic survey will be re-recorded occupying the same stations as before. If the interpretation of the seismic amplitudes anomalies is correct, the large amplitude anomaly interpreted as DNAPL should be diminished significantly or be gone.

Hanford 200 W Area

The Plutonium Finishing Plant at USDOE Hanford Site utilized quantities of carbon tetrachloride (CCl_4) as a heavy liquid separator during plutonium recovery operations. Between 1955 and 1973 an estimated 360-580K liters of CCl_4 were discharged into waste facilities at 200 West area. The study area is adjacent to the 216-Z-9 crib which was one of the disposal sites (Fig. 8). At this location there is a 10 sq km plume of highly concentrated CCl_4. Borehole data indicates that the highest DNAPL concentrations have accumulated at the contact of the Pleistocene Hanford Fine with the Plio-Pleistocene and at the contact of the Plio-Pleistocene with an underlying caliche zone.

Four seismic reflection profiles were collected to encompass the Z-9 crib (Fig. 8). These profiles are designated lines Z-9-1, Z-9-2, Z-9-3, and Z-9-4. The data were acquired using a 120-channel Geometrics Strataview recording system and a vibrator source. The group and shot intervals were one meter. Lines were laid to tie wells with high concentrations of CCl_4 in the vicinity of the crib (Fig. 8). For velocity control and seismic modeling purposes P-wave and S-wave VSPs were recorded in three wells.

The first step in the interpretation was to determine which reflections correspond to thePlio/Pleistocene and the Caliche zone. The significance of these reflections is that the DNAPL tends to accumulate in the vicinity of these two events in the subsurface. A VSP was acquired in well 299-W15-32 to establish a tie between the geologic units and the seismic events present in the survey data.
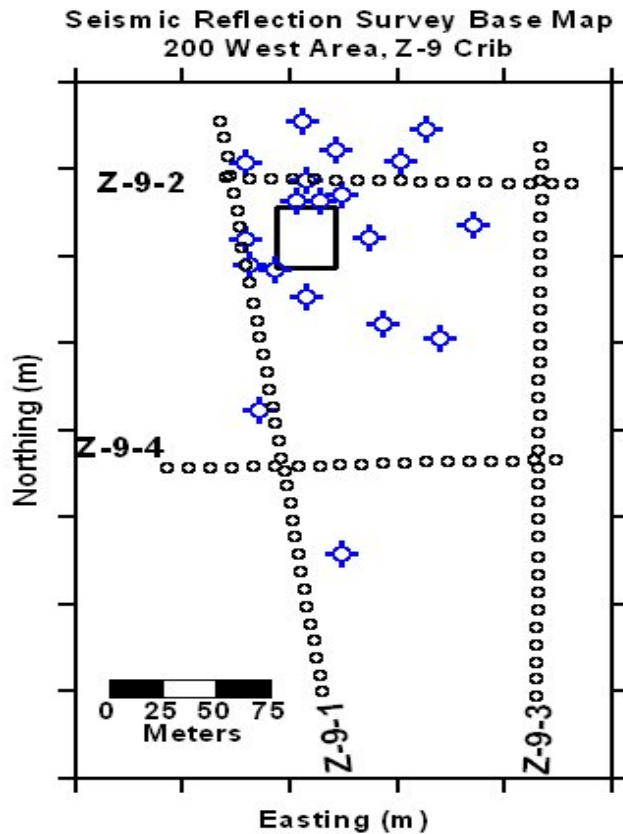
Figure 8. Location plat for the Hanford 200 W
area. The small rectangular box is the Z-9 crib.

Seismic Line Z-9-1

Seismic Line Z-9-1 was shot from south-southeast to north-northwest along the west side of
the crib (Fig. 7). Two events were interpreted on the line. The green event at approximately 0.120
s corresponds to the top of the Plio/ Pleistocene boundary (Base of the Hanford Fine). The event is
somewhat discontinuous, but is mappable. The average depth to this unit is approximately 37 meters.
The data indicates incisement of this event by the overlying Pleistocene Hanford Fine unit. The
Hanford fine interval on line Z-9-1 has a channel incised into the Plio-Pleistocene from shot point
(SP) 183 to SP 241. The depth of incisement is approximately 16 ms (3-4 meters).

The blue event is the top of Caliche marker. It roughly corresponds to the Pliocene age
Ringold Formation and based on interpretation of the geologic data is most likely the surface upon
which the DNAPL is resting. It is a high amplitude event that is mappable over the entire survey
interval. Amplitude intensity drops in the vicinity of the channel from SP 166-196   Downcutting by
the overlying Plio/Pleistocene appears to have occurred from SP 163 to the end of the line making

the south end of the line structurally higher. However, the overall dip direction is from north to south.

The Plio/Pleistocene interval displays a rather uniform parallel reflection pattern indicative of deposition in a rather quiet lower energy environment. This unit more than likely was a fill unit consisting of silts and clays deposited during a quiet period. The Upper boundary displays erosional truncation with events being truncated by the overlying Pleistocene Hanford Fine. Downlap occurs on to the top surface of the Plio/Pliestocene.

Seismic Line Z-9-2

Seismic Line Z-9-2 was shot from east to west along the northern boundary of the crib area and intersects lines Z-9-1 and Z-9-3 (Fig. 8). The green marker (Fig. 8) is the top of the top of the Plio/ Pleistocene boundary. The event on this line is more continuous than on Line Z-9-1. Average depth to this unit is 36 meters. A channel is incised into the Plio/ Pleistocene boundary from 109-165. The horizon is generally flat across the line. Interval characteristics of the Plio/Pleistocene are similar to line Z-9-1 displaying flat lying concordant internal events. The top of Caliche (Blue event, Fig. 8) is a high in amplitude and continuous across the section.

Seismic Line Z-9-3

Seismic Line Z-9-3 is a north-south trending profile east of the crib and intersects Z-9-2 and Z-9-3. The green event is the Plio/Pleistocene (Fig. 9). The event is discontinuous, but mappable along the line. Average depth to the Plio/Pleistocene is approximately 34-35 meters. A significant channel is present down cutting into the Plio/Pleistocene from SP 236-406. The channel has a maximum thickness of 21ms (approx. 33 meters). From SP 279-311 the channel has removed almost the entire Plio/Pleistocene section and is close to eroding through the caliche zone into the Ringold Formation as well (Fig. 9). The green event has an overall dip direction from south to north of approximately 3 meters. The Blue event is the top of Caliche. The event is continuous and high in amplitude across the section. Approximately 3-4 meters of dip from north to south occur along the line.

Seismic Line Z-9-4

Seismic Line Z-9-4 is an east-west trending line south of the crib and intersects lines Z-9-1 and Z-9-3. The green event (Fig. 10) is the top of the Plio/Pleistocene and dips from east to west approximately 10 meters. The event is very discontinuous, but still mappable along the line. A channel is incised beginning at SP 252 and continues west until the end of the line. The maximum thickness of the channel is 34 ms (11 meters) and occurs near the end of the line at SP 113. The Blue event (Fig. 10) is the top of Caliche. This horizon dips from east to west very gently. The amplitude of the event is high and is mappable the entire length of the line. The Pleistocene channel has almost completely removed the overlying Plio/ Pelistocene unit and is in close proximity to the Caliche along the west end of the line.

Structural Interpretation

Structure contour maps were generated on two horizons, the Plio/ Pleistocene (green event, and the top of Caliche (blue event). The channel downcutting into the Plio/Pleistocene surface is readily apparent on the structure contour map on top of the Plio/Pleistocene (Fig. 11). A structural high is located on line Z-9-1 at SP 340. The surface dips off to the north and northeast from this high. A structural high also exists on the southern end of Line Z-9-3. Most of the relief on this surface is from the erosion by the channel in the overlying unit bisecting the map area. The movement of DNAPL in the subsurface is more dependent on structure than groundwater flow. Given the location of the source of entry for the solvents into the ground, the most likely flow direction for DNAPL would be to the north and northeast of the Plio/Pliestocene high present on line Z- 9-1 (Fig. 11).
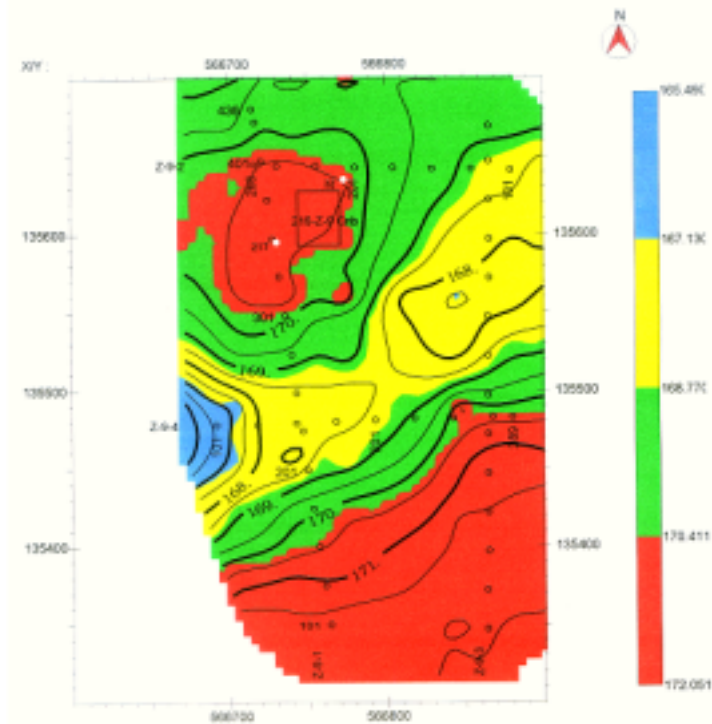

Figure. 11 Structure contour map Top of Plio/Pleistocene. Contours are in meters above sea level.

A similar structural picture is observed on the top of Caliche map (Fig.12). A structural high exists on line Z-9-1 near the tie with Line Z-9-2. The geologic characteristics of this surface would indicate that this would be the most likely candidate surface for the DNAPL to collect. Any DNAPL flowing along this surface, assuming that crib is the source, would gravity flow to the north and northeast.

Figure 12. Structure contour map top of Caliche.
Contours are in meters above sea level.

DIRECT DETECTION OF DNAPL

At the 200 W Area carbon tetrachloride is present both in the vadose zone as well as in the water table. The solvent is found throughout the 65-meter thick vadose zone (Rohay, 1994). Rohay (1994) states that the highest concentrations of CCl_4 are associated with the Hanford fine and the Plio-Pleistocene units located approximately 35-40 meters below ground surface.

Based upon the modeling for this report an amplitude anomaly should be present along the Plio/Pleistocene and top of Caliche horizons where DNAPL is present. Each line was taken through a standard processing scheme to generate the sections used for structural interpretation. Additional processing was undertaken to enhance amplitude variations in the stacked data. The amplitude of each sample was replaced with 10 raised to the power of the scaled and balanced sample amplitude. The result is that high amplitude values are exponentially boosted whereas low amplitude values are suppressed.

Z-9-1 Enhanced Amplitude Stack

Figure 13 is the enhanced amplitude stack for Z-9-1. Significant amplitude anomalies exist on line Z-9-1 along the top of Caliche event. An anomaly exists from SP 379-426 at 121 ms, from SP 346-360 at 123 ms and from SP 270 –306 at 125 ms. A minor anomaly exists from SP 128-164 at 123 ms.   Amplitude increases are seen in the interval between the Plio/Pleistocene (green event) and the Caliche (blue event) boundaries.

According to Rohay (1994) well 299-W15-217 had the highest measured CCl_4 concentrations in the area (37,817 ppb) at a depth of 34.7 meters at the Plio/Pleistocene event (green). This corresponds to one of the significant amplitude anomalies present on line Z-9-1 from SP 346-360 at approximately 120 ms (Fig.13).

Z-9-2 Enhanced Amplitude Stack

Figure 14 is the enhanced amplitude stack for Z-9-2. Significant amplitude increases exist on Z-9-2 from SP 114-152, SP 154-219, and SP 226-261 at approximately 127 ms. This corresponds to near the top of Caliche reflector. Amplitudes in general are significantly higher along this profile and are vertically more extensive than on Z-9-1.   These amplitudes along with the areal extent suggest that significant DNAPL is present along this surface.

Well 299-W15-218 projects into an amplitude anomaly on Line Z-9-2 at SP 209 and well 299-W15-219 projects into the end of an anomaly on Z-9-2 at SP 260. Wells 299-W15-218 and 299-W15-219 yielded CCl_4 concentrations of 15,794 ppb at 33.5 m and 11,688ppb at 34.9m respectively. These depths are in good agreement with line Z-9-2 for the interval between the Plio/Pliestocene and the top of Caliche reflectors.

Z-9-3 Enhanced Amplitude Stack

Figure 15 is the enhanced amplitude stack for Z-9-3. Z-9-3 is located east of the crib area. A major increase in amplitude exists on Z-9-3 from SP 351-400 along the top of Caliche reflector. To the south along the line an amplitude increase exists from SP 114-204 within the Ringold Formation, but above the water table. The significance of this amplitude anomaly is not known at this time.

Z-9-4 Enhanced Amplitude Stack

Figure 16 is the enhanced amplitude stack for Z-9-4. The line is located to the south of the crib area. Z-9-4 displays no amplitude anomalies along the line at any horizon. This would indicate that there is no DNAPL present along the profile.

Integrated Interpretation

Plio/Pleistocene

Amplitude maps were created on two horizons, the Plio/Pleistocene and the top of Caliche reflectors. Amplitude values along these surfaces were picked and contoured to allow interpretation of the data for DNAPL distribution.

Figure 17 is a contour map of the amplitudes at the top of the Plio/Pleistocene horizon. Modeling of this horizon shows that in the presence of CCl_4 (DNAPL), the amplitude along this event should be reduced, i.e. a dim-out. Areas of dim-out are represented by the green and blue colored areas. In general, these areas are located under the crib, to the east of the crib, and west of the crib. These reduced amplitude zones are located in structural lows along the surface of the Plio/Pleistocene (Fig. 11).
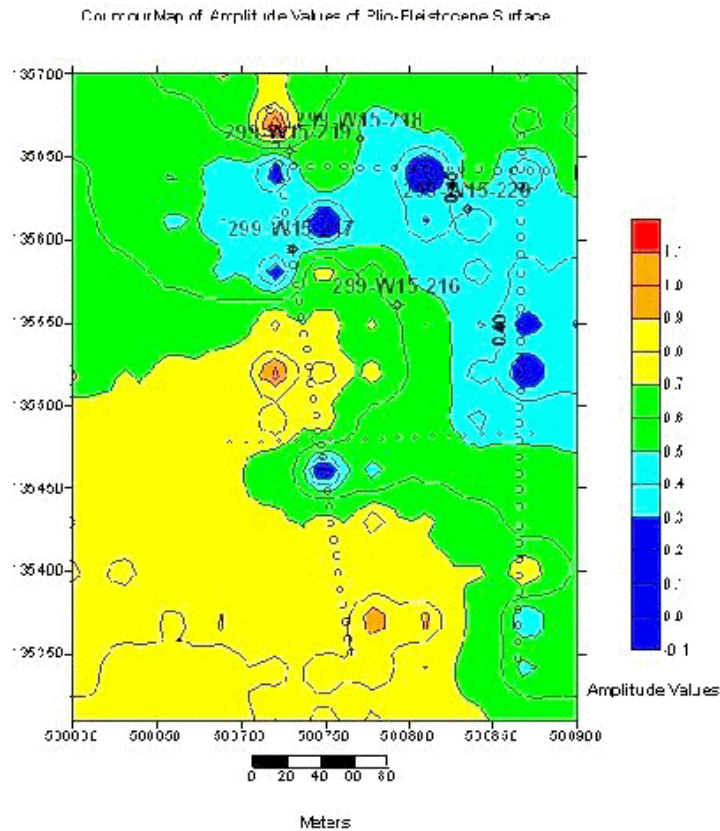
Figure 17. Contour map of amplitude values Top of the Plio/Pleistocene horizon. Contour values are arbitrary.

Top of Caliche

Figure 18 is the amplitude map on the top of the Caliche reflector. Based on the modeling, a high amplitude event at the Top of the Caliche is associated with the presence of DNAPL. Amplitude values on the caliche surface represented by the red and yellow are the highest along line Z-9-2 and are projected to run to the north of the area. A large area represented by the area colored green also displays an increase in amplitude over background. Under assumption that an amplitude increase in indicates DNAPL, CCl$_4$ in free-phase has collected along the top of Caliche in this location. No evidence exists for the presence of DNAPL south and east of the crib in the area colored blue at this horizon.
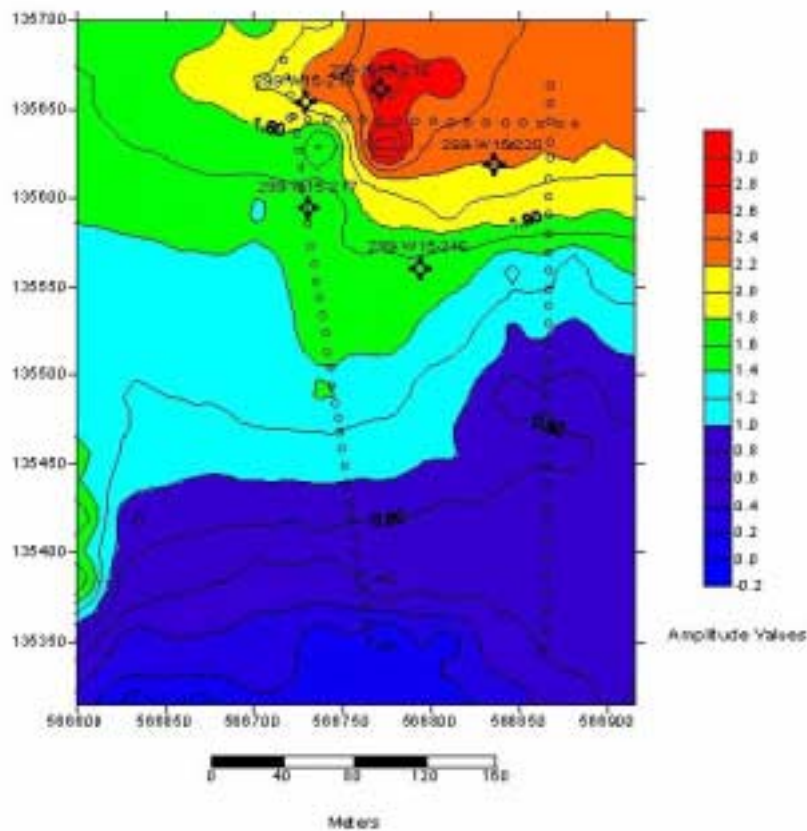
Figure 18.   Contour map of the amplitude values top of Caliche surface. The contour values are arbitrary.

Figure 19 is a contour map of the average concentration of CCl_4 in the Plio/Pleistocene—Caliche interval in the crib area. Information from five wells, 299-W15-216, 299-W15-217, 299-W15-218, 299-W15-219, and 299-W15-220 were collected and averaged over the interval represented by the Plio/Pleistocene and gridded. Areas of high concentration of CCl_4 in the interval are represented by red values. Areas of low concentration are in shades of blue. The northwest area of the map (the area encompassing wells 299-W15-217, 299-W15-218, 299-W15-219) falls within the zone of high concentration. This agrees well with the amplitude anomaly maps of the top of Plio/Pleistocene (Fig. 17) and top of Caliche (Fig. 18). The area directly under well 299-W15-218 is an overlay on all maps.
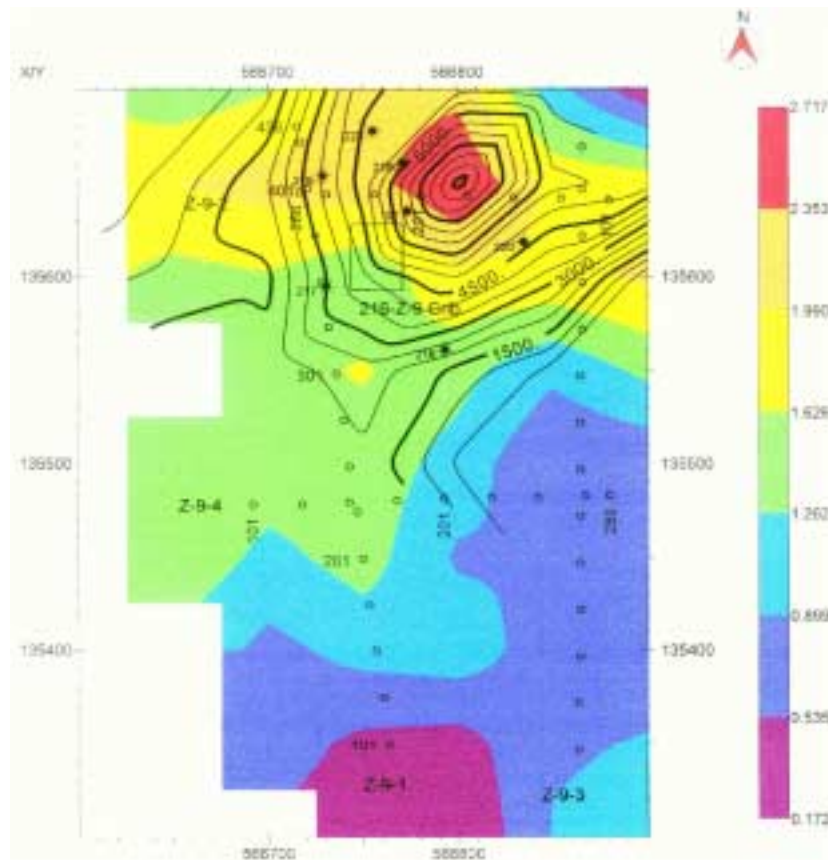
Figure 19. Contour map of the average concentration of CCl_4 in the Plio/Pleistocene—Caliche interval in the crib area. Contour interval in ppmv. Shaded contours are amplitude at top of Caliche (arbitrary values).

The seismic data showing the position of free-phase CCl_4 in the subsurface agrees well with the known concentrations based on well data. Modeling results indicate that where carbon tetrachloride exists a dim-out in amplitudes should be present along the Top of the Plio/Pleistocene event and an increase in amplitude should be present along the top of Caliche surface.

Based on the close agreement of the seismic and the well data, a prediction of the location of free-phase CCl_4 can be made with reasonable confidence at the caliche event. The event when

enhanced yields a distinctive anomaly that can be mapped with high confidence.

6.0   APPLICATION

In summary, seismic reflection surveying and seismic reflection AVO analysis are noninvasive techniques that, under certain circumstances, provide a means of 1) mapping subsurface lows where DNAPL might accumulate, and 2) directly detect the presence of free- phase DNAPL in the subsurface. This approach significantly reduces the cost of site characterization and prevents cross-contamination between aquifers by reducing the number of monitoring wells.

The seismic reflection survey is the only subsurface remote sensing method capable of providing dense spatial sampling of subsurface material properties at depths 30 feet and greater. In addition, emerging technology, such as application of the AVO techniques described and proposed herein, present the possibility of directly detecting the presence of subsurface DNAPL. These technologies will result is a significantly more extensive understanding of the subsurface characteristics and properties of waste sites, which will lead to an efficient and cost-effective cleanup of groundwater.

Furthermore DNAPLs can be identified more quickly by seismic reflection surveying because of the dense subsurface sampling and direct detection potential. This information will provide a better basis for developing groundwater models used to design remediation strategies. The delineation of contaminant plumes and the placement of monitoring wells will be facilitated, thereby saving time and money over a method using the random installation of wells.

Application of seismic reflection techniques to subsurface site characterization will reduce public and occupational health risks because, as a noninvasive technique, there will be less exposure to hazardous subsurface contaminants. Field crews will assume less risk. There is less disturbance of aquifers and fewer opportunities for inadvertently spreading contaminants.

Site remediation is always negotiable and site-specific. The more defensible the characterization information, the better the chance to obtain regulatory approval.

The geophysical techniques proposed are well established in the petroleum industry where they have been applied in an extensive range of geological settings. It remains to implement the technology in the hydrogeological and subsurface contamination remediation industries.

References

Aki, K. and Richards, P.G., 1980, Quantitative Seismology: W. H. Freeman and Co., San Francisco, 932 p.

Allen, J.L. and Peddy, C.P., 1993, Amplitude variation with offset: Gulf Coast studies: SEG

Geophysical Developments Series No. 4, Society of Exploration Geophysicists, Tulsa, OK, 111 p.

Bortfield, R., 1961, Approximation to the reflection and transmission coefficients of plane longitudinal and transverse waves: Geophysical Prospecting, v. 9, p. 485-502.

Castagna, J.P. and Backus, M. M., eds., 1993, Offset-dependent reflectivity - Theory and practice: SEG Investigations in Geophysics No. 8, Society of Exploration Geophysicists, Tulsa, OK, 345 p.

Castagna, J.P., Batzle, M.L., and Eastwood, R.L., 1985, Realtionship between compressional and shear-wave velocities in clastic siscate rocks, Geophysics, v. 50, p. 551-570.

Koefoed, O., 1955, On the effect of Poisson's ratios of rock strata on the reflection coefficients of plane waves: Geophysical Prospecting, p. 381-387.

Ostrander, W.J., 1984, Plane-wave reflection coefficients for gas sands at nonmormal angles of incidence: Geophysics, v. 49, p. 1637-1648

Rohay, V.L., 1994, 1994 conceptual model of the carbon tetracloride contamination in the 200west area at the Hanford Site,WHC-SD-EN-TI-248, Westinghouse Hanford Comapny, Richland, Washington.

Shuey, R.T., 1985, A simplification of the Zoeppritz equations: Geophysics, v. 50, p. 609-614.

Smith, G.C. and Gidlow, P.M., 1987, Weighted stacking for rock property estimation and detection of gas: Geophysical Prospecting, v. 35, p. 993-1014.

Verm, R. and Hilterman, F., 1995, Lithology color-coded seismic sections: The calibration of AVO crossplotting to rock properties: The Leading Edge, v. 14, n. 8, p. 847-853.

Waddell, M.G, Temples, T.J., and Domoracki, W.J., 1997, Using high-resolution reflection seismicto image free-phase DNAPLs at the M-area, Savannah River Site (Abstract): Ann. Mtg.Am.Assoc. Petroleum Geologists, Dallas, TX.

Waters, K.H., 1981, Reflection Seismology: A Tool for energy resource exploration, John W,Wiley and Sons, Inc.

Zoeppritz, K., 1919, Uber reflexion und durchgang seismischer wellen durch Unstetigkerlsflaschen: Berlin, Uber Erdbebenwellen VII B, Nachrichten der Koniglichen Gesellschaft der Wissenschaften zu Gottingen, math-phys. K1., p. 57-84.
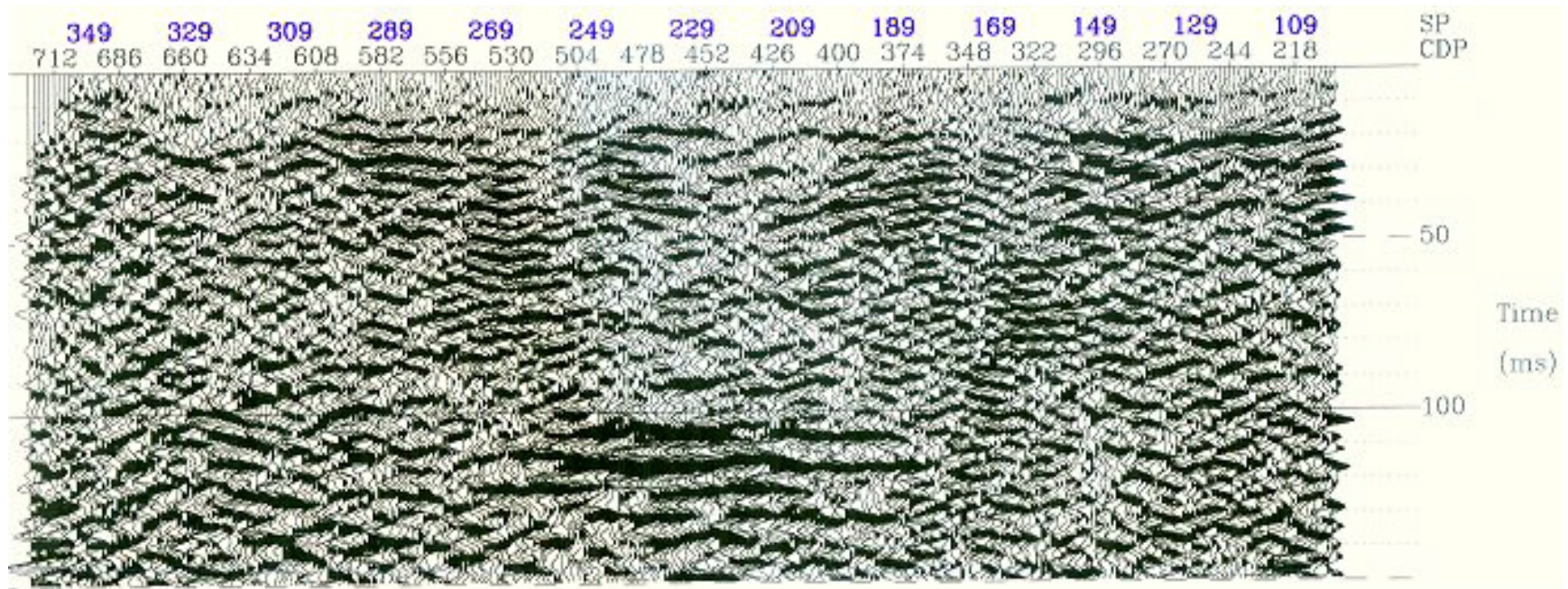
Figure 3. Seismic line DUS-1 Savannah River Site. Notice the only reflector occurring at 110 to 120 ms between shot points 189 and 269. Every other trace displayed. SP spacing is 2 ft.
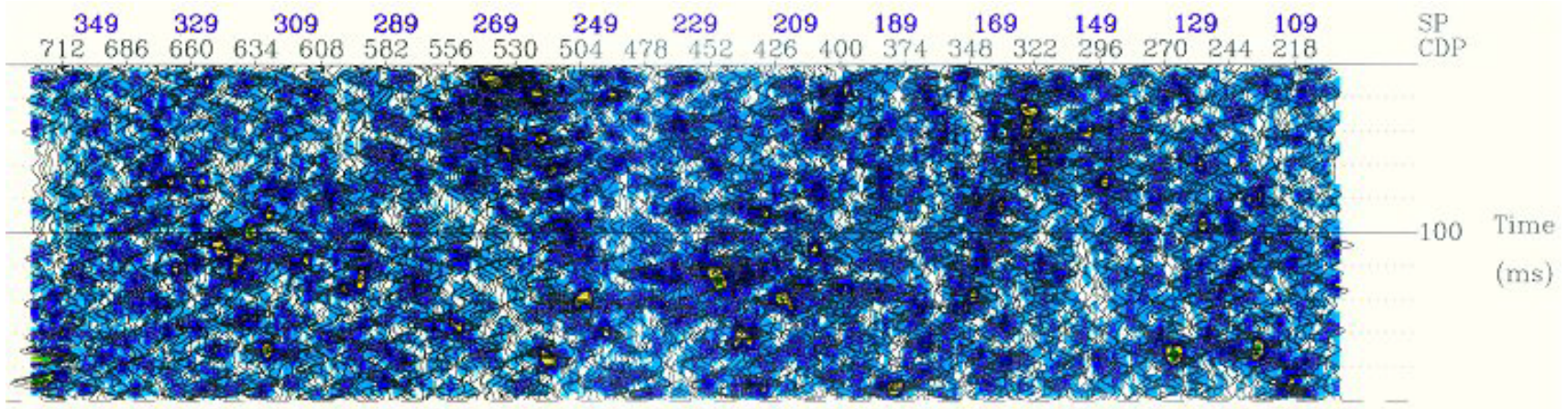
Figure 4. Seismic line DUS-1 near offset stack. The highest concentration of DNAPL is reported in the well labeled "nasty" Fig.2 which located at shot point (SP) 210. Every other trace plotted. Amplitude envelope display.
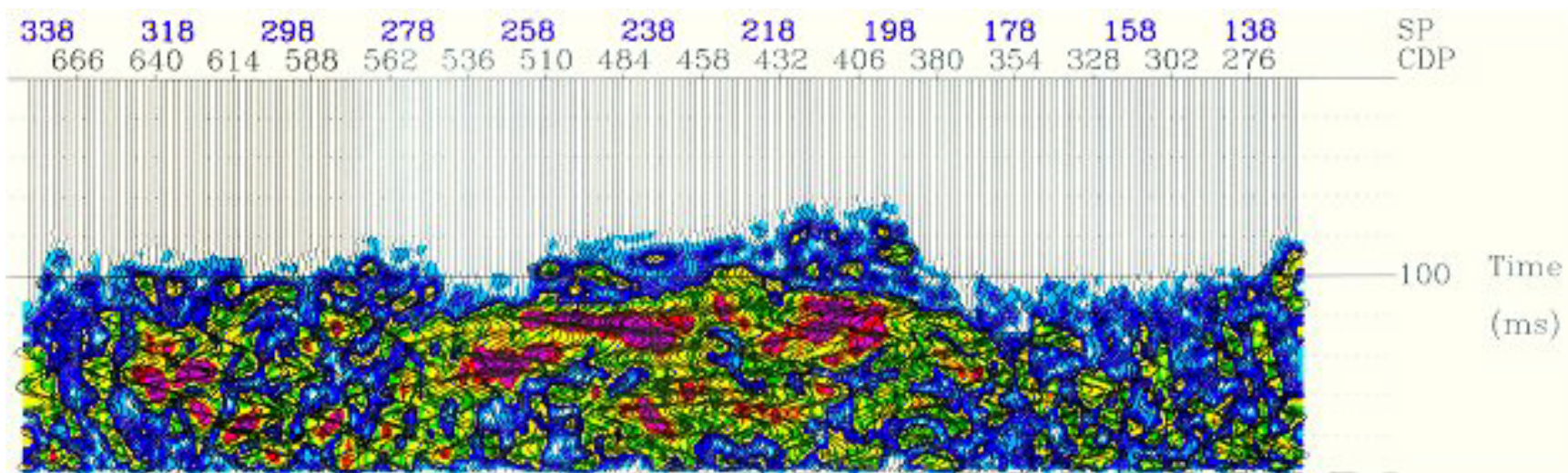
Figure 5: Seismic line DUS-1 far offset stack. If the models are correct, there should not be an amplitude anomaly on the near offset stack (Fig. 4) but only on the far offset stack. Between shot points (SP) 200 and 269 at 110 ms there is an amplitude anomaly. The well label "nasty" (Fig. 2) is located at shot point 210 which is located in the large amplitude anomaly. Every other trace plotted. Amplitude envelope display.
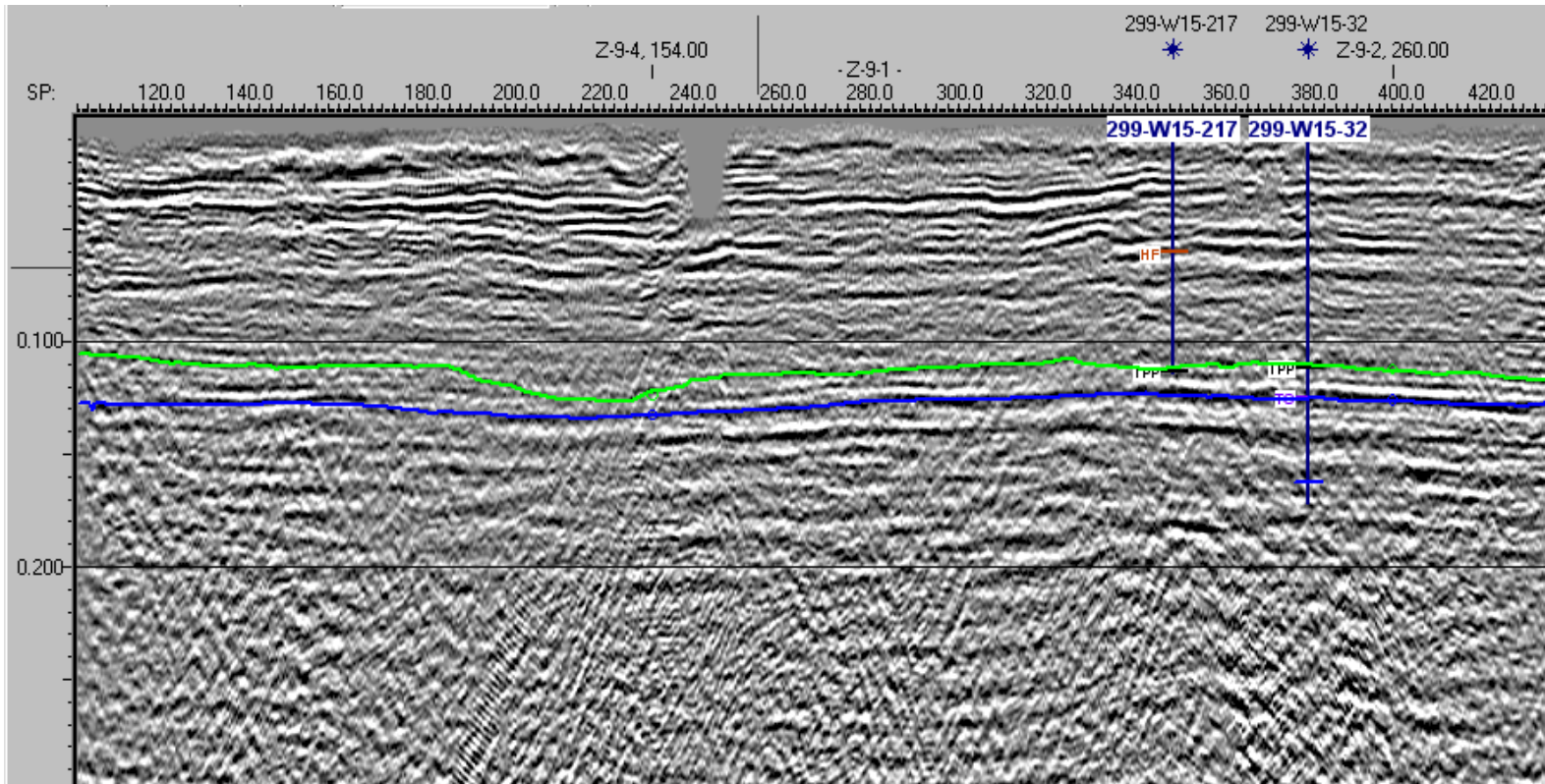
Figure 7.   Seismic Line Z-9-1. Green horizon is top of Plio/Pleistocene. Blue horizon is top of Caliche.
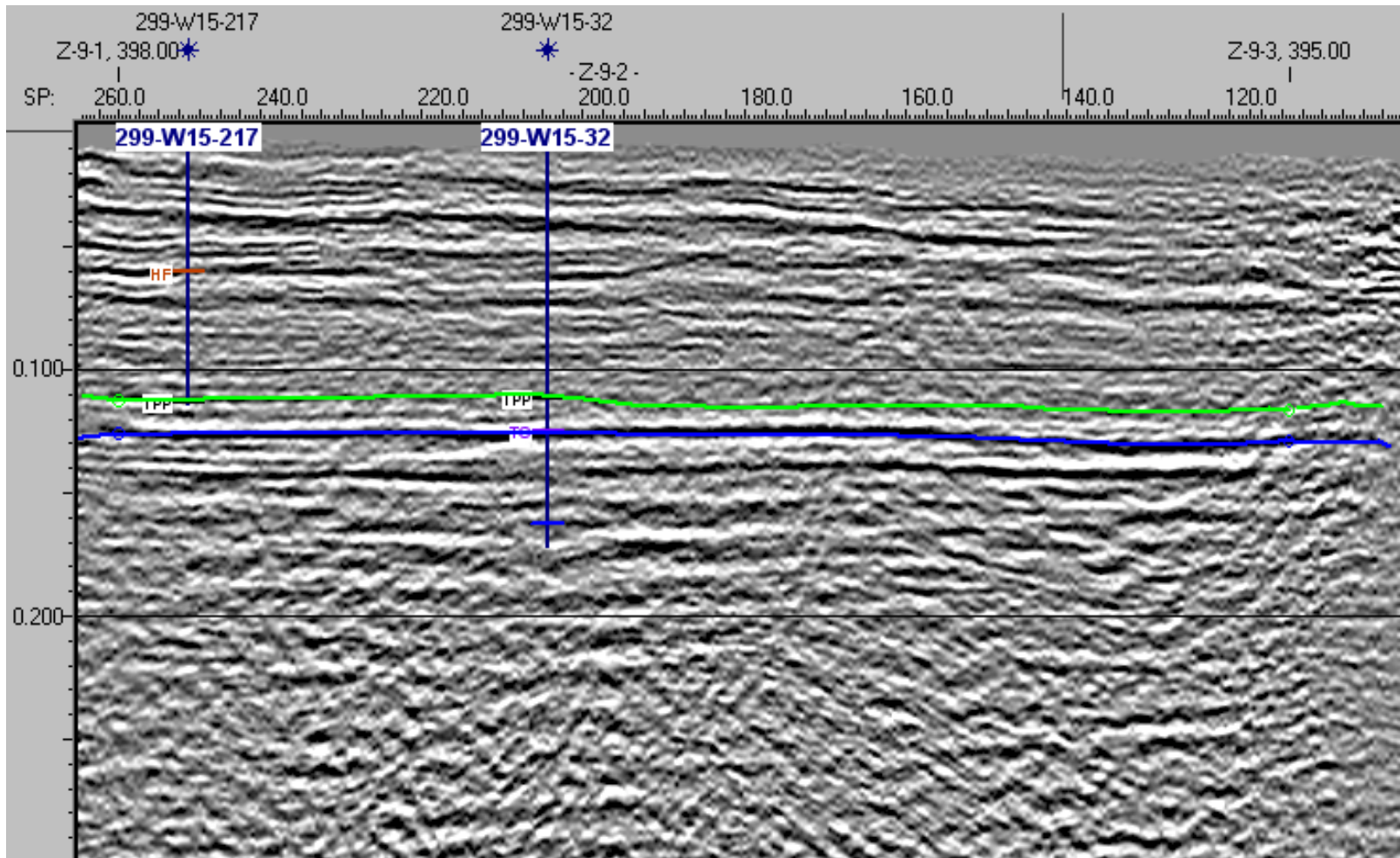
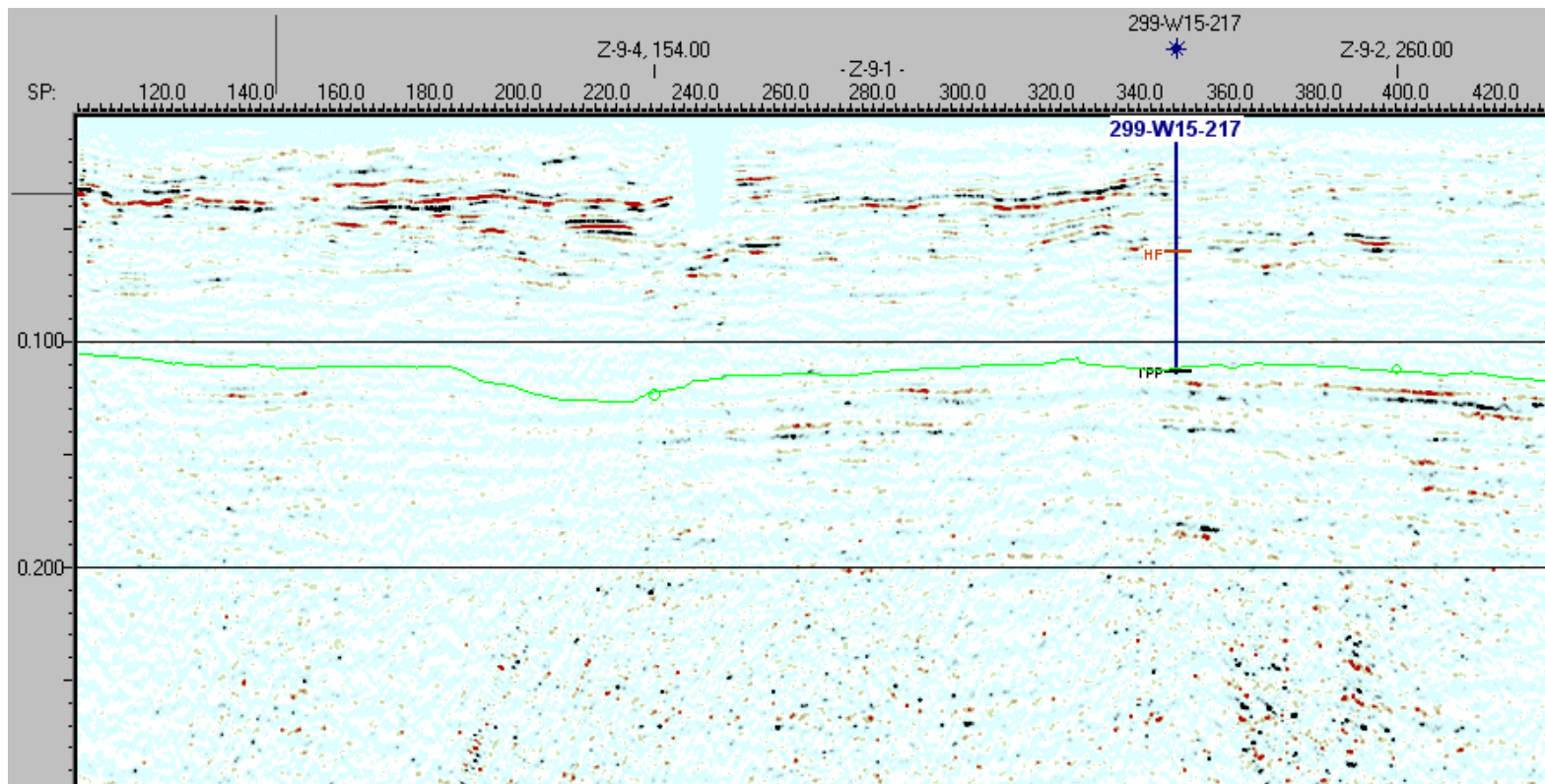Figure 8. Seismic Line Z-9-2 Green horizon is top of Plio/Pleistocene. Blue horizon is top of Caliche.
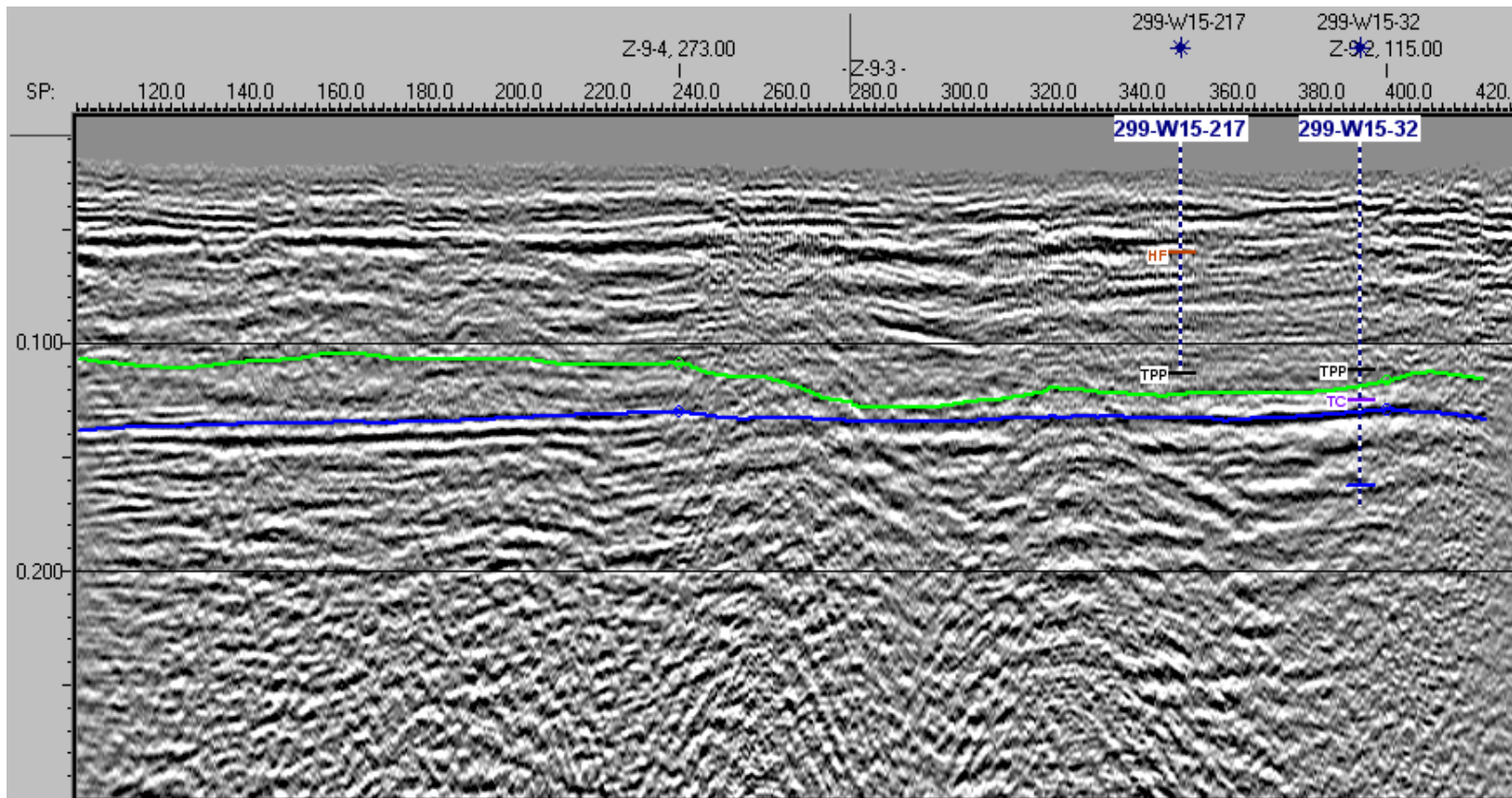
Figure 9. Seismic Line Z-9-3   Green horizon is top of Plio/Pleistocene. Blue horizon is top of Caliche.
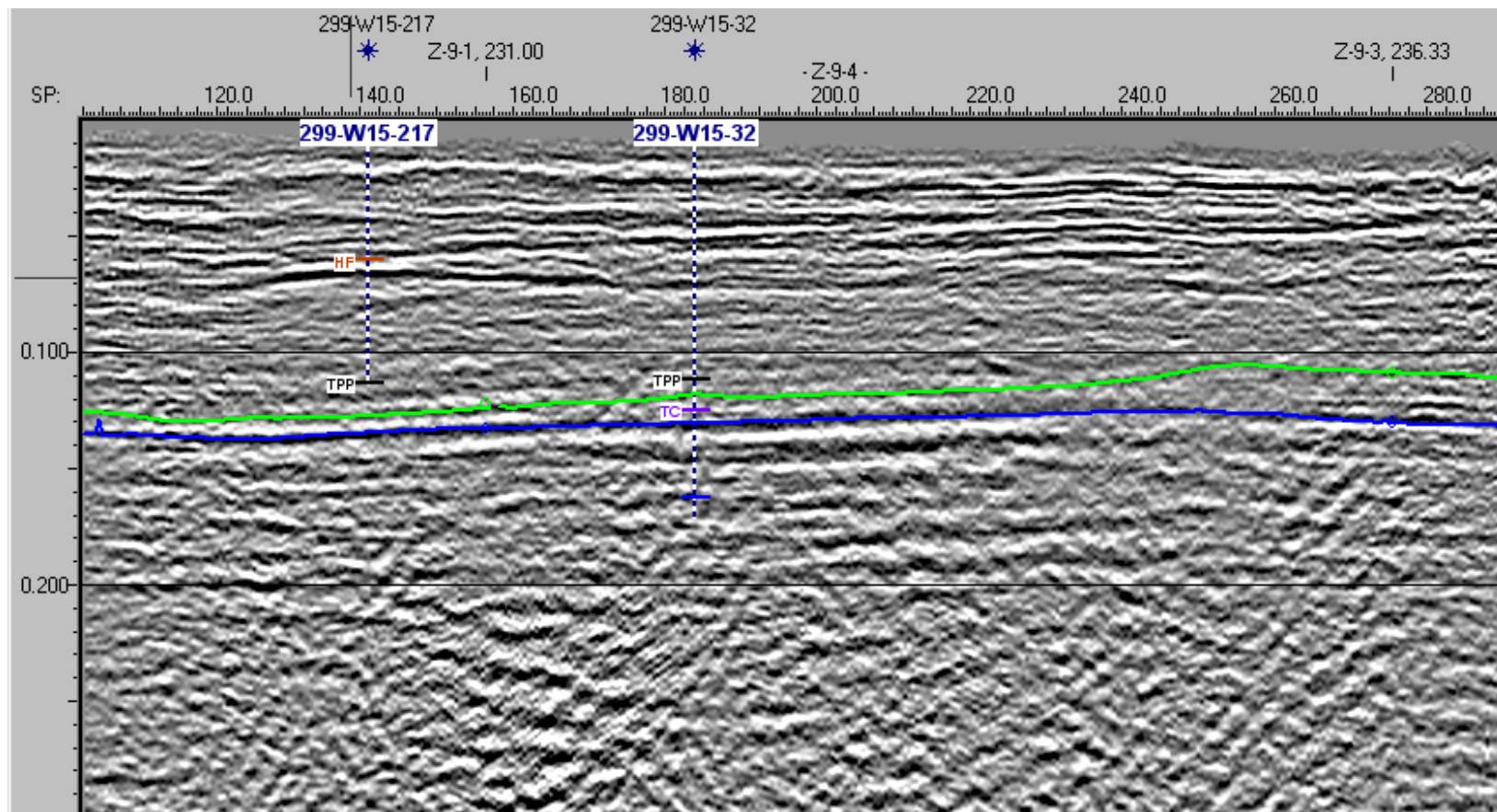
Figure 10. Seismic Line Z-9-4   Green horizon is top of Plio/Pleistocene. Blue horizon is top of Caliche.

Figure 13. Enhanced amplitude plot of Line Z-9-1. Areas in black are positive amplitudes, areas in red are negative amplitudes. Green Horizon is top of Plio/Pleistocene.
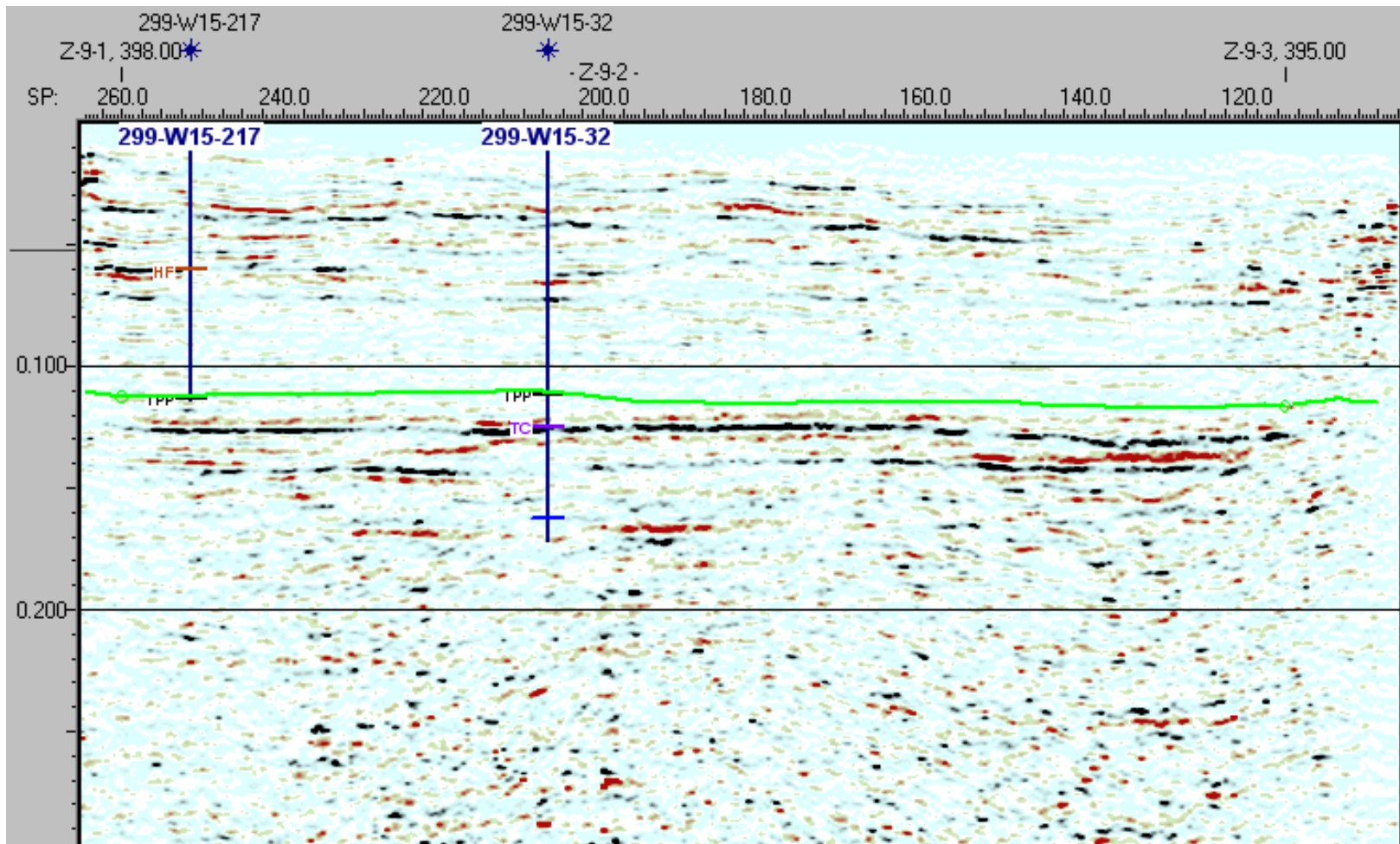
Figure 14. Enhanced amplitude plot of Line Z-9-2. Areas in black are positive amplitudes, areas in red are negative amplitudes. Green Horizon is top of Plio/Pleistocene.
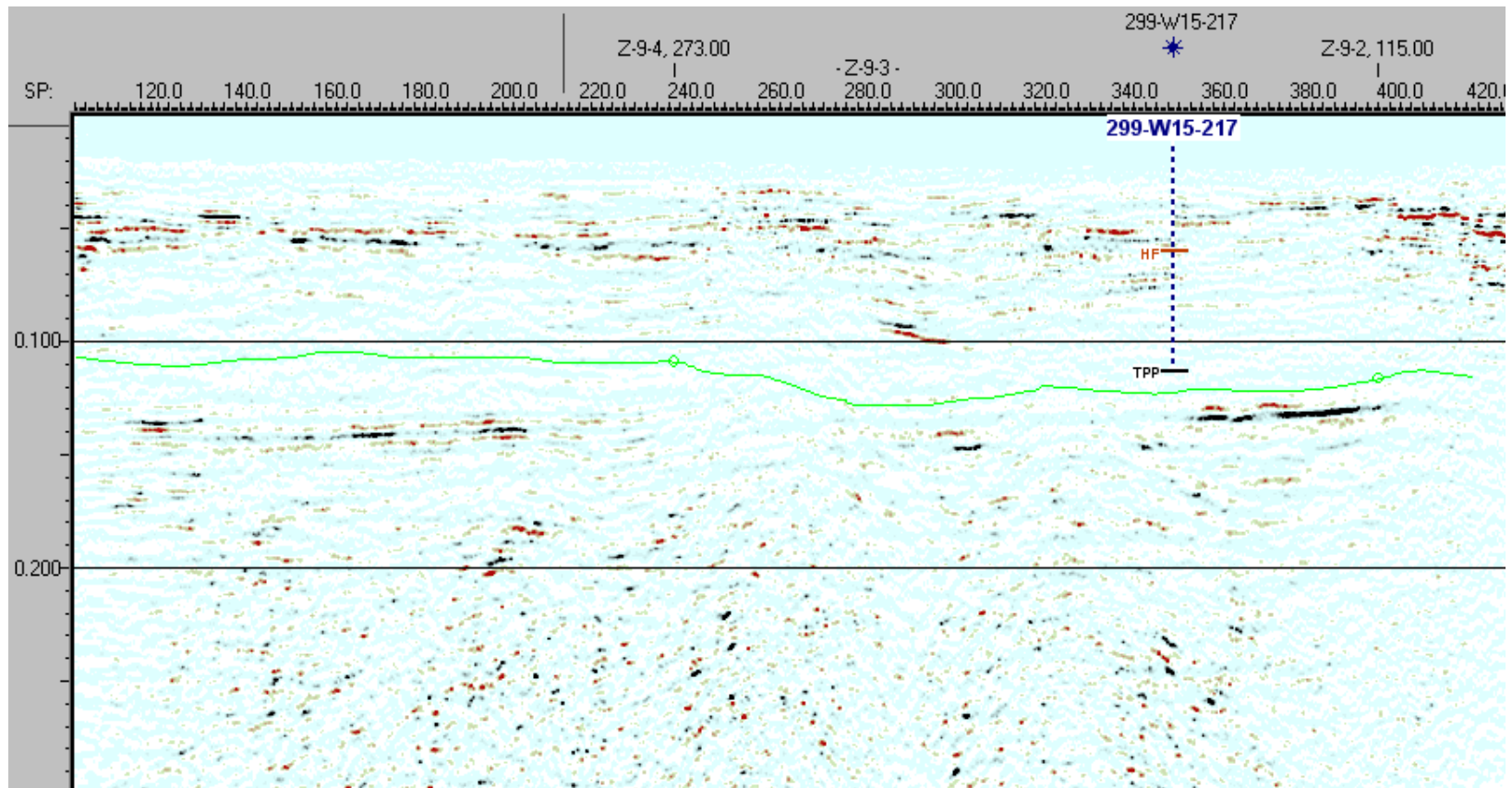
Figure 15. Enhanced amplitude plot of Line Z-9-3. Areas in black are positive amplitudes, areas in red are negative amplitudes. Green Horizon is top of Plio/Pleistocene.
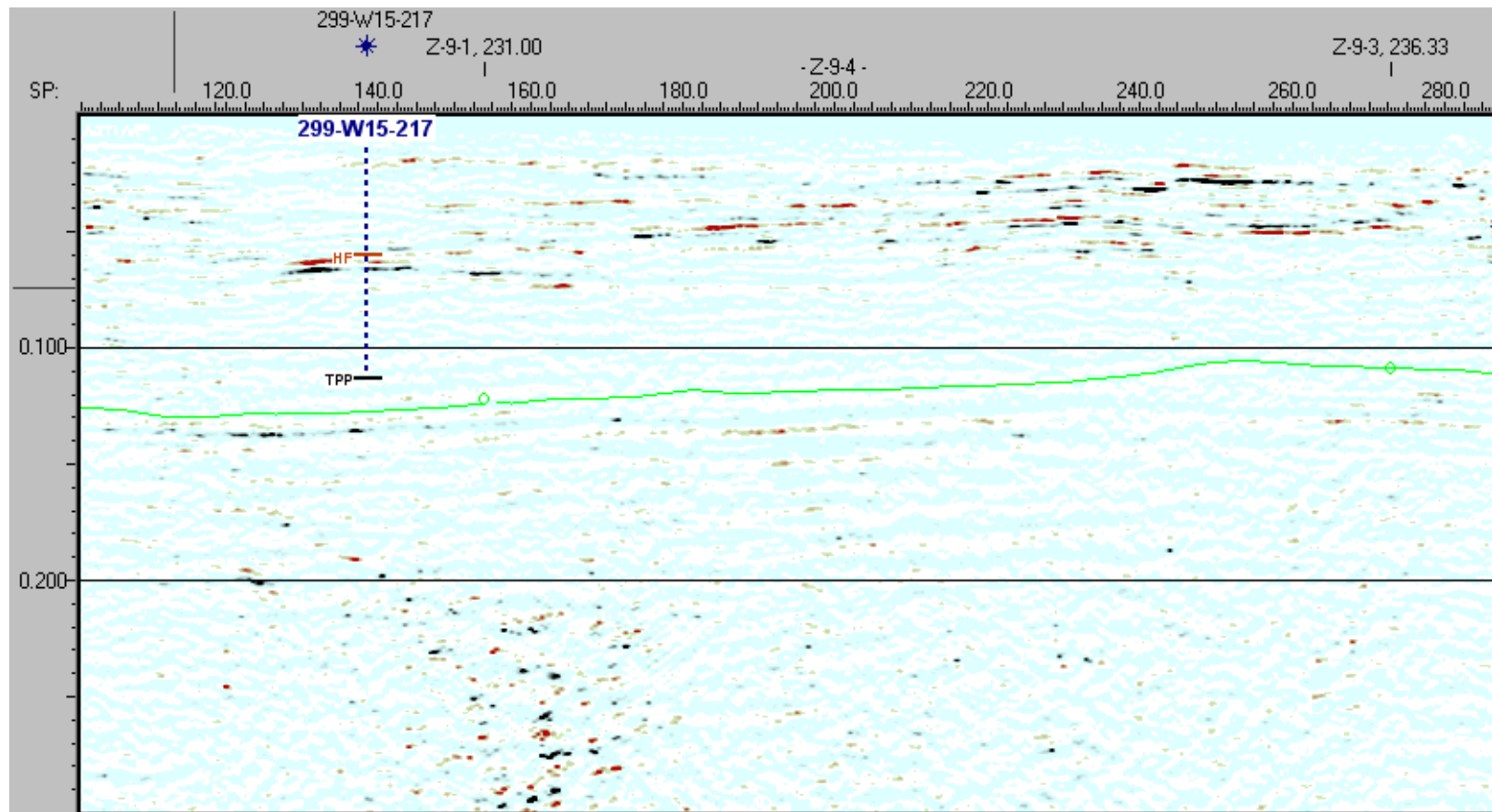
Figure 16. Enhanced amplitude plot of Line Z-9-4. Areas in black are positive amplitudes, areas in red are negative amplitudes. Green Horizon is top of Plio/Pleistocene.